Journal of Materials Chemistry B

PAPER

View Article Online
View Journal | View Issue

Cite this: J. Mater. Chem. B, 2015, 3, 6081

Folic acid-conjugated organically modified silica nanoparticles for enhanced targeted delivery in cancer cells and tumor *in vivo*†

Feng Yin,‡[a] Butian Zhang,‡[a] Shuwen Zeng,[ab] Guimiao Lin,[c] Jinglin Tian,[c] Chengbin Yang,[a] Kuan Wang,*[d] Gaixia Xu*[be] and Ken-Tye Yong*[a]

Received 2nd April 2015,
Accepted 17th June 2015

DOI: 10.1039/c5tb00587f

www.rsc.org/MaterialsB

In this work, we report the synthesis of dye-loaded and folic acid (FA)-conjugated organically modified silica (ORMOSIL) nanoparticles as targeted optical nanoprobes for *in vitro* and *in vivo* imaging. The dye-loaded ORMOSIL (ORM^D) nanoparticles are synthesized by a facile aqueous phase (oil-in-water microemulsion) approach and they have an average size of 30 nm. We observed that the functionalization of FA onto the particle surface led to a strong cellular uptake of FA-conjugated ORM^D nanoparticles for pancreatic cancer Miapaca-2 cells and hepatoma SMMC7721 cells with FA receptor overexpression. Such a trend is not observed for 293T cells and breast cancer MCF7 cells as these cells possess low-expression of the FA receptor. The *in vivo* imaging studies demonstrate that FA-ORM^D nanoparticles are preferentially accumulated in tumor sites. Histological studies reveal that no-ill effects are observed in the major organs of treated mice when compared to the untreated ones. Because of the facile synthesis process, high specificity for tumor targeting and low toxicity of FA-ORM^D nanoparticles, significant potential for early-cancer detection application is expected.

Introduction

Noninvasive bioimaging techniques provide a powerful tool to visualize the in-depth penetration of tissues and enable the visualization of complex physiological and pathological processes such as disease progression and therapeutic intervention. A broad range of imaging methods (*e.g.* computerized tomography (CT), magnetic resonance imaging (MRI), positron emission tomography (PET), photoacoustic imaging, and optical imaging) have been developed for various disease detection and monitoring at the preclinical and clinical phases. Each of these methods has its strength and weakness in terms of sensitivity, resolution, specificity, scanning speed, instrumental cost and potential toxicity effects. The conventional CT and MRI techniques used in clinical diagnosis are effective for whole organism imaging, but they still need improvements in sensitivity and specificity for imaging the tissue/cellular level.[1] The PET technique can be used to overcome these limitations since it is able to provide a three dimensional image analysis of functional processes in the body. However, the scanning speed of PET is relatively slow and its spatial resolution is intrinsically limited.[2,3] As a promising complementary method to these imaging modalities, optical imaging is a high-speed, low-cost imaging technique with high spatial and temporal resolution due to their advanced development of fluorescence microscopy (*e.g.* laser scanning microscopy, multiphoton imaging, *etc.*) which can be used for sensitive *in vivo* imaging.[4] Using a biomarker-conjugated contrast agent, one can use optical imaging to acquire high resolution images ranging from tissue to the cellular level with high specificity. Biomarkers such as proteins, peptides, aptamers and small biomolecules are commonly used as homing agents for targeted delivery. Nowadays, the development of optical imaging has enabled the monitoring of distribution and metabolism of drug molecules,[5–7] infectious disease processes,[8,9] neurodegenerative disease progression,[10] and even tumor growth and metastasis.[11–14]

Currently, many optical imaging technologies are being developed toward both basic and clinical applications. The main challenge of employing optical imaging for clinical application

[a] School of Electrical and Electronic Engineering, Nanyang Technological University, Singapore 639798, Singapore. E-mail: ktyong@ntu.edu.sg
[b] CINTRA CNRS/NTU/THALES, UMI 3288, Research Techno Plaza, 50 Nanyang Drive, Border X Block, Singapore, 637553, Singapore
[c] The key lab of Biomedical Engineering and Research Institute of Uropoiesis and Reproduction, School of Medical Sciences, Shenzhen University, Shenzhen, 518060, China
[d] Nanomedicine Program and Institute of Biological Chemistry, Academia Sinica, Nankang, Taipei 115, Taiwan. E-mail: wangk@gate.sinica.edu.tw
[e] Key Laboratory of Optoelectronics Devices and Systems of Ministry of Education/Guangdong Province, College of Optoelectronic Engineering, Shenzhen University, Shenzhen, P. R. China. E-mail: xugaixia@szu.edu.cn

† Electronic supplementary information (ESI) available. See DOI: 10.1039/c5tb00587f

‡ These authors contributed equally to this work.

lies in the successful fabrication of biocompatible optical probes with good colloidal stability in complex physiological fluids. More importantly, these probes should be designed in such a way that they can be removed from the body after performing their programmed task either through an excretion or degradation process. Organic fluorophores and fluorescent proteins[15,16] are traditional optical probes which are widely used for *in vitro* imaging research. However, their use for *in vivo* imaging is significantly impeded by several disadvantages like insufficient photostability under long-term irradiation, poor colloidal stability in biological fluids, a complex bioconjugation process and potential toxicity *in vivo*.[17,18] Integrating organic fluorophores into nanoparticles is an excellent approach to address the problems mentioned above and it will aid in opening a new avenue for *in vivo* optical imaging applications.[19–22] Benefiting from their controllable surface properties, size, and high chemical robustness, nanoparticles have received great attention in the biomedical fields and they have been applied for a variety of applications such as drug delivery,[23–25] optical imaging[26,27] and cancer therapy.[20,28–30] Dye encapsulated or conjugated polymer nanoparticles[31–33] are expected to be relatively nontoxic considering the biocompatibility of some Food and Drug Administration (FDA) approved polymer molecules, but many of the polymer particles are susceptible to deformation or disassembly due to pH and polarity change in solvents,[34,35] which may result in fast release of organic dyes in biological fluids and negatively impact the overall performance as an optical contrast agent. Such challenges can be solved by the rational design of embedding organic dyes in silica nanoparticles. More importantly, silica nanoparticles have been considered as suitable nanoprobes for *in vivo* optical imaging[36,37] due to their distinct advantages,[38–44] which includes: (i) their size, morphology and porosity are highly controllable; (ii) the optical transparent properties of the particles allowing them to cover a wide range of emission spectra by encapsulating various fluorophores and quantum dots; (iii) the low toxicity of the silica material makes them physically and chemically robust in biological fluids; (iv) by varying the silica precursors during the modification process, the organically modified silica (ORMOSIL) nanoparticles can be fabricated with different functional groups (hydroxyl/amine/thiol/carboxyl) for bioconjugation; and (v) as the silica nanoparticles are benign to most living organisms and categorized as "Generally Recognized As Safe" (GRAS) by the U.S. FDA, the silica nanoparticles are considered to be highly biocompatible for *in vivo* applications.

In this study, we developed a facile and efficient strategy to synthesize the folic acid (FA)-functionalized and dye-entrapped ORMOSIL nanoparticles and successfully employed them as optical probes for pancreatic tumor targeted imaging. In our approach, the oil-in-water microemulsion system is specifically used to synthesize ORMOSIL nanoparticles encapsulated with the organic dyes. Subsequently, folic acid (FA) is conjugated to the silica nanoparticles as a homing agent. Our fluorescence imaging and flow cytometry results showed that a much higher cellular uptake of FA conjugated silica (FA-ORM^D) nanoparticles is observed upon comparing to the unconjugated ones in Miapaca-2 cells and other FA-receptor-positive cancer cells (SMMC7721 cells). To examine the specificity of FA-ORM^D nanoparticles for *in vivo* imaging, we treated the pancreatic cancer xenograft model with the FA-conjugated ORMOSIL nanoparticles by tail vein injection. A strong fluorescence signal is observed specifically at the tumor site after 1 hour of treatment and maintained up to 1 day. In addition, the toxicity and biodistribution of FA-ORM^D nanoparticles are investigated by using both *in vitro* and *in vivo* models. The cell viability of the treated Miapaca-2 culture cells is maintained over 80% even at a high dosage of 1 mg mL^{-1} for 24 hours. From histological studies of treated mice, FA-ORM^D nanoparticles caused no abnormalities in the major organs. After 2 weeks, the animals are sacrificed and their major organs are harvested for fluorescence imaging analysis. Fluorescence signals are detected from the liver and spleen suggesting that a good fraction of nanoparticles are located in these two organs, which is consistent with other reports. Herein, we have developed an efficient, specific and nontoxic optical probe for cancer imaging.

Materials and methods

Chemicals and reagents

Vinyltriethoxysilane (VTES, 679275), N^1-(3-trimethoxysilylpropyl) diethylenetriamine (DETA, 413348), Dimethyl sulphoxide (DMSO, D8418), Tween-80 (P4780), 1-butanol (B7906), 4-(dicyanomethylene)-2-methyl-6-(*p*-dimethylaminostyryl)-4*H*-pyran (DCM, 410497), folic acid (FA, F8758), *N*-(3-dimethylaminopropyl)-*N*′-ethylcarbodiimide (EDC, 39391), Sodium hydroxide (NaOH, S8045), *N*-hydroxysuccinimide (NHS, 130672) and 3-(4,5-dimethylthiazol-2-yl)-2,5-diphenyltetrazolium bromide (MTT, M2128) were purchased from Sigma Aldrich. 18.2 MΩ cm Deionized (DI) water obtained from a Milli-Q Integral 5 system was used in all experiments.

Synthesis and purification of DCM dye-entrapped organically modified silica (ORMSIL) nanoparticles

To synthesize the ORMOSIL nanoparticles, a microemulsion system was prepared by mixing 200 mg of Tween-80, 600 μL of 1-butanol, 200 μL of DMSO and 20 mL of DI water. For preparing DCM dye-entrapped ORMOSIL nanoparticles, 1 mg mL^{-1} DMSO solution of DCM dye was used instead of the pure DMSO. After stirring for 20 min, 200 μL of VTES was added to the solution and the mixture was stirred for another 1 h. After this, 20 μL of DETA was injected and the mixture was stirred for 20 h. Then the solvents were dialyzed in DI water for 2 days. Before using these prepared nanoparticles, 5 mL of their solution were dialyzed against DMSO until agglomeration occurred. Subsequently, the solution of silica particles was centrifuged at 12 000 rpm and the precipitation was redissolved in 2 mL of DI water.

Conjugation of DCM-entrapped ORMOSIL nanoparticles with folic acid (FA)

1 mg mL^{-1} FA was activated using 10 mM EDC and 10 mM NHS in pH 6 buffer solution (a molar ratio of FA/EDC/NHS = 1 : 2 : 2). After vortexing for 30 min, the pH of the solution was raised to

8.5 by adding NaOH. Afterwards, 4.5 mL of the above solution and 750 μL of the dye-entrapped ORMSIL nanoparticle solution was mixed in 15 mL of phosphate-buffered saline (PBS). The reaction mixture was vortexed for 4 h and kept at 4 °C overnight. Then FA conjugated ORMOSIL nanoparticles were collected by centrifugation and redissolved in 750 μL of water under sonication. For maintaining the stability of the nanoparticle dispersion, FA-ORM^D nanoparticles are freshly prepared for experimental use.

Characterization of ORMSIL nanoparticles

Transmission electron microscopy (TEM) images were obtained by using a JEOL model JEM-2010 transmission electron microscope at an acceleration voltage of 200 kV. The specimens were prepared by drop-casting the sample dispersion onto a carbon coated 300 mesh copper grid (Carbon Type-B, Ted Pella, Inc.). After coating the samples on the grid, uranyl acetate solution (2%, 10 μL) was dropwise added on the grid for negative staining. The UV-visible absorption spectra were obtained using a spectrophotometer (Shimadzu UV-2450). The hydrodynamic size distribution profile and the zeta potential of ORMSIL nanoparticles were measured using a particle size analyzer system (90 Plus, Brookhaven Instruments). For Fourier transform infrared (FTIR) spectroscopy, the samples were dried under vacuum overnight and their FTIR spectra were acquired using a Shimadzu spectrometer.

Tumor cell line and culture

Human pancreatic cancer cell line Miapaca-2 (CRL-1420, American Type Culture Collection) and human embryonic kidney cell line 293T (CRL-11268, American Type Culture Collection) were maintained in Dulbecco's modified Eagle's medium (DMEM, Hyclone), human hepatoma cell line SMMC7721 (3115CNCB00263, China Center for Type Culture Collection) was maintained in RPMI-1640 medium (Hyclone) and human breast cancer cell line MCF7 (HTB-22, American Type Culture Collection) was maintained in Eagle's Minimum Essential Medium (EMEM, Hyclone). All these kinds of medium were supplemented with 10% (v/v) fetal bovine serum (FBS, Hyclone) and penicillin/streptomycin (100 μg mL^{-1}, Gibco). Cells were cultured at 37 °C in a humidified atmosphere with 5% CO_2.

Flow cytometry

For the flow cytometry assay, treated Miapaca-2 cells, 293T cells, SMMC7721 cells and MCF7 cells were washed twice with phosphate-buffered saline (PBS) and harvested by trypsinization. The DCM dye was served as the luminescent marker (a filter set for PerCP-Cy5.5 was applied) to determine the transfection efficiency quantitatively. The samples were analyzed using a FACScalibur flow cytometer (Becton Dickinson, Mississauga, CA).

Cell imaging and viability studies

For cell imaging, Miapaca-2 cells and 293T cells were treated with ORM, ORM^D or FA-ORM^D nanoparticles and incubated for 4 h. Before imaging, cells were washed with PBS and fixed with 5% formaldehyde. For the cell viability test, the MTT (3-(4,5-dimethylthiazol-2-yl)-2,5-diphenyltetrazolium bromide, Sigma) assay was performed. Miapaca-2 cells were seeded in 96-well plates at a density of 5×10^3 cells per well and cultured for 24 h. Then eight sets were treated with different concentrations of ORM, ORM^D or FA-ORM^D nanoparticles with one set as an untreated control. After incubation for 24 h, MTT (5 mg mL^{-1}, 20 μL) in PBS was added and the cells were incubated for another 4 hours at 37 °C with 5% CO_2. After this, the medium with MTT was removed and 150 μL DMSO was then added to solubilize the precipitate with 5 min gentle shaking. Absorbance was measured using a microplate reader (Bio-Rad) at a wavelength of 490 nm. The cell viability was obtained by normalizing the absorbance of the sample well against that from the control well and expressed as a percentage, assigning the viability of non-treated cells as 100%. Assays were performed in triplicate and the results were averaged.

Animal studies

Preparation of pancreatic tumor-bearing mice. Athymic nude mice (BALB/cASlac-nu, female) at five to six weeks of age were obtained from Shanghai Slac Laboratory Animal Co. Ltd, Chinese Academy of Sciences, with licensing number of SCXK-2007-0005. Mice were maintained in an isolated biosafety facility for specific pathogen free (SPF) animals with bedding, food and water. All operations were carried out in accordance with the National Standard of Animal Care and Use Procedures (20080820)[45] at Laboratory Animal Center of Shenzhen University, Guangdong Province, People's Republic of China (the permit number is SZU-HC-2014-02).[46] For preparation of pancreatic tumor-bearing mice, athymic nude mice were raised for one or two weeks to adapt to the new environment and then were injected with 1×10^7 *in vitro* propagated Miapaca-2 cells (Miapaca-2 cells were trypsinized, harvested and resuspended in DMEM, 100 μL volume of each) subcutaneously in the lower flank of mice. Tumor volumes were measured by calipers (accuracy of 0.02) every other day and calculated using the equation $V = (L \times W^2)/2$, in which L and W refer to the larger and smaller dimensions. The *in vivo* optical imaging experiments were performed until the volume reached 200–300 mm^3 (in approximately 10 to 15 days post transplantation of cells).

***In vivo* imaging.** When the tumor reached an appropriate volume of 200–300 mm^3, the mice were injected with 200 μL of FA-ORM^D nanoparticles (1 mg mL^{-1}) by tail vein injection (10 mg kg^{-1}, n = 3). After injection, mice were anesthetized with isoflurane. The induction concentration was 5% isoflurane/1 L O_2, and the maintenance concentration was 2–3% isoflurane/1 L O_2. Once the mice were properly anesthetized, they were imaged at indicated time points to monitor the accumulation of FA-ORMOSIL-DCM nanoparticles in tumors using the IVIS Lumina II small animal *in vivo* optical imaging system (Caliper). In this study, the scanning wavelength range between 500 and 950 nm was used for *in vivo* imaging.

Preparation of paraffin section histological analysis. For histological experiments, organ tissues were collected on the final day and fixed in 4% buffered formalin-saline at room

temperature for 24 h. Following this, tissues were embedded in paraffin blocks and paraffin sections of 4 μm thickness were mounted on a glass slide for hematoxylin and eosin (H&E) staining. The H&E staining slices were examined under a light microscopy (Olympus BX51).

Results and discussion

Synthesis and characterization of ORMSIL nanoparticles

Silica nanoparticles have been applied in various biomedical research fields due to their biocompatibility, nontoxicity and tunability in optical properties. In a typical synthesis process, silica nanoparticles are produced in a water-in-oil microemulsion system where corrosive nonpolar solvents are used and this generally requires tedious purification steps. Unlike the traditional methods, we have synthesized these ORMSIL nanoparticles in a simple aqueous phase (oil-in-water microemulsion) system. As shown in Fig. 1A, the TEM images show high monodispersed ORM^D nanoparticles with an average particle size of 30 nm. The hydrodynamic diameter of ORM^D nanoparticles is estimated to be 33.4 ± 4.02 nm by using the dynamic light scattering (DLS) technique (Fig. 1D). The zeta potential value of the purified ORM^D nanoparticles is determined to be 9.99 ± 0.42 mV, indicating a successful surface modification by amino-group terminated silica precursors. The absorption spectra of ORM^D nanoparticles combine the features originated from the DCM dye spectra and the spectra of the ORM nanoparticles (Fig. 1B). The DCM dye has poor solubility in DI water and it cannot be directly solubilized in biological fluids. With the addition of DMSO, the DCM dye can be dispersed in DMSO/DI mixtures but show weak fluorescence signals and they tend to aggregate quickly. In this work, the DCM dye is dissolved in the Tween 80/water/DMSO microemulsion. Subsequently, the growth of silica nanoparticles is carried out on the oil–water interface and it is expected to encapsulate the hydrophobic DCM dye in the oil droplet interface. The synthesized ORM^D nanoparticles preserved the bright fluorescence signals of the DCM dye (~25% QY) and they were stable in DI water for weeks, which provided the evidence that DCM dyes were entrapped in ORM^D nanoparticles rather than in the solvent. The estimated loading capacity of DCM is 7.36 μg mg^{-1}. Also, the long-term stability of the ORM^D dispersion suggests that the encapsulated dye did not leak out from the silica matrix, otherwise insoluble aggregates can be detected. Upon comparing to the spectra of DCM dyes in DMSO solution, the ORM^D nanoparticles show broader and blue-shifted emission spectra (Fig. 1C). The difference in their emission spectra is attributed to the conformation change in the DCM molecules[34,47] where they are entrapped in the silica matrix. On the other hand, the supernatant acquired in purification steps (free dyes in the solution) exhibited similar photoluminescence (PL) spectra when compared to the free DCM dyes. This in fact signifies that the PL change is caused by the entrapped dyes in silica nanoparticles rather than the effects from the solvents.

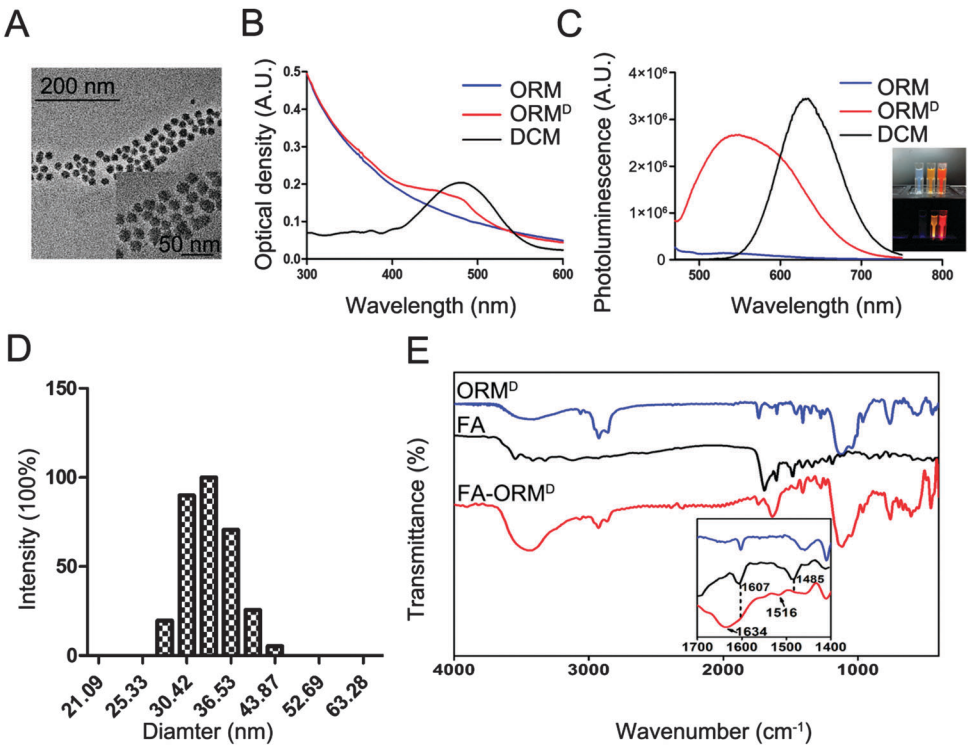

Fig. 1 Characterization of ORMOSIL nanoparticles. (A) TEM images of ORM^D nanoparticles. (B) Absorption and (C) photoluminescence (PL) spectra of ORM nanoparticles, ORM^D nanoparticles (in water) and the DCM dye (in DMSO). Inset images are the corresponding solutions under natural and UV light. (D) Hydrodynamic size distribution of ORM^D nanoparticles with an average size centered at 33.4 ± 4.02 nm. (E) FTIR spectra of FA, ORM^D nanoparticles and FA conjugated ORM^D nanoparticles.

Fluorescence imaging of Miapaca-2 cells

Folate targeting is an emerging approach for cancer theranostics.[48,49] A folic acid-receptor (FR) has been extensively considered as a tumor marker because of the selectively high expression of the FR on the surface of many human cancer cells[50–52] (*e.g.* ovarian, lungs, breast, kidneys, brain and pancreatic cancer cells). Folic acid (FA) or vitamin B_9 displays high affinity for the FR, which is captured by the FR from the extracellular environment and was transported inside the cell within the recycling endosomal compartments.[53] Therefore, we functionalized the fluorescent ORM^D nanoparticles with FA to target the pancreatic cancer cells (Miapaca-2 cells) *via* FA-FR-mediated endocytosis. The preparation process of ORM^D and FA-ORM^D nanoparticles are shown in Scheme 1. The zeta potential value of the purified FA-ORM^D nanoparticles is determined to be 6.23 ± 2.64 mV. The conjugation is examined by comparing the FTIR spectra of ORM^D nanoparticles with that of the FA-ORM^D nanoparticles. From Fig. 1E, the emergence of the bands at 1634 and 1516 cm^{-1} is attributed to amide I and amide II bonds[54–56] within FA and formed between FA and amino group-functionalized silica nanoparticles. The successful conjugation is further confirmed by the appearance of the FA characteristic peaks (1607 and 1485 cm^{-1}) in the spectra of ORM^D nanoparticles.

In Fig. 2, the selective uptake of different ORMOSIL nanoparticle formulations by Miapaca-2 cells is monitored by fluorescence microscopy. Miapaca-2 cells are separately treated with 50 μg mL^{-1} ORM, ORM^D or FA-ORM^D nanoparticles for 4 hours before they are examined under the microscope. In Fig. 2D, a strong uptake of FA-ORM^D nanoparticles (red fluorescence signals) by Miapaca-2 cells is observed. As a comparison, very weak fluorescence signals are observed for Miapaca-2 cells treated with unconjugated ORM^D nanoparticles, ORM nanoparticles and PBS buffer (Fig. 2A–C). To further confirm that the nanoparticles are internalized *via* the FA-mediated endocytosis, Miapaca-2 cells were pre-treated with 30 μg mL^{-1} FA for 30 minutes to block the FR on the cellular surface and then the samples were incubated with FA-ORM^D nanoparticles for 4 hours (Fig. 2E). As expected, no significant fluorescence signals were obtained from the FA treated cells because the excess free folic acid molecules are competitively bound to the FR. These *in vitro* fluorescence imaging results suggest that the conjugation of FA to the particles can effectively increase the cellular uptake of ORM^D nanoparticles.

Flow cytometry analysis of Miapaca-2 cells treated with ORMOSIL nanoparticles

As shown in Fig. 3, the transfection efficiency of different ORMOSIL nanoparticles in Miapaca-2 cells is quantitatively evaluated by flow cytometry. Miapaca-2 cells are separately treated with 50 μg mL^{-1} ORM, ORM^D or FA-ORM^D nanoparticles for 4 hours before measuring the fluorescence intensity by flow cytometry. Fig. 3A shows the representative plots of the fluorescence intensity in Miapaca-2 cells. The corresponding transfection efficiency and average fluorescence signals are depicted in Fig. 3B and C, respectively. The cells treated with FA-ORM^D nanoparticles exhibit strongest fluorescence signals and their corresponding transfection efficiency is estimated to be 92 ± 0.37%, which is much higher than that of the cells treated with ORM^D nanoparticles (the transfection efficiency is 30 ± 0.15%). In contrast, weak fluorescence signals are detected from the cells pre-treated with FA followed by incubation with FA-ORM^D nanoparticles (the transfection efficiency is 5 ± 0.64%). The above differences demonstrate the essential role of FA for the efficient uptake of ORM^D nanoparticles in Miapaca-2 cells. As negative controls, the cells treated with ORM or PBS show almost no fluorescence signals from this analysis study. These results are in good agreement with the cell fluorescence imaging analysis and further confirm the specificity of FA-ORM^D nanoparticles for targeting Miapaca-2 cells.

Fluorescence imaging of human embryonic kidney 293T cells

To further assess the tumor targeting ability of FA-ORM^D nanoparticles, we incubated 293T cells with 50 μg mL^{-1} ORM^D and FA-ORM^D nanoparticles for 4 hours and examined them under the microscope (Fig. 4) and flow cytometry (Fig. 5). 293T cells are isolated from human embryonic kidneys and are transformed with large T antigen. They are normal human cells and have a low expression of the FR.[47,54,55] Therefore, 293T cells served as negative controls to verify the specific tumor targeting efficiency of FA-ORM^D nanoparticles. In Fig. 4C, the red fluorescence signals indicated a relatively low amount of the uptake of ORM^D nanoparticles in 293T cells. As a comparison,

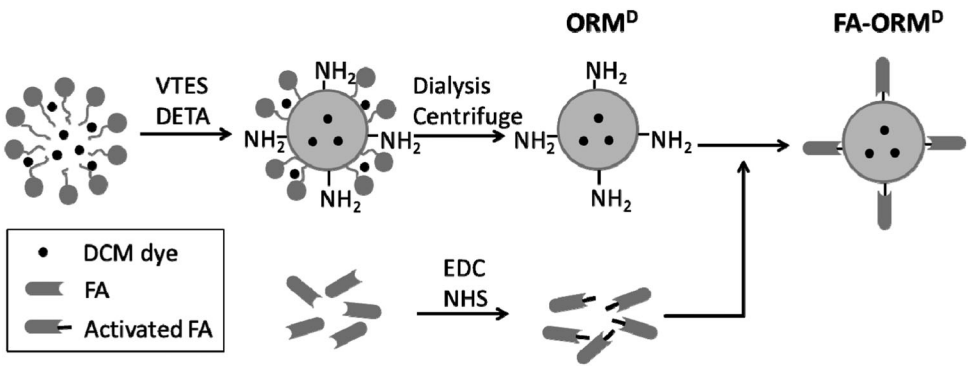

Scheme 1 Representative scheme showing the preparation of ORM^D and FA-ORM^D nanoparticles.

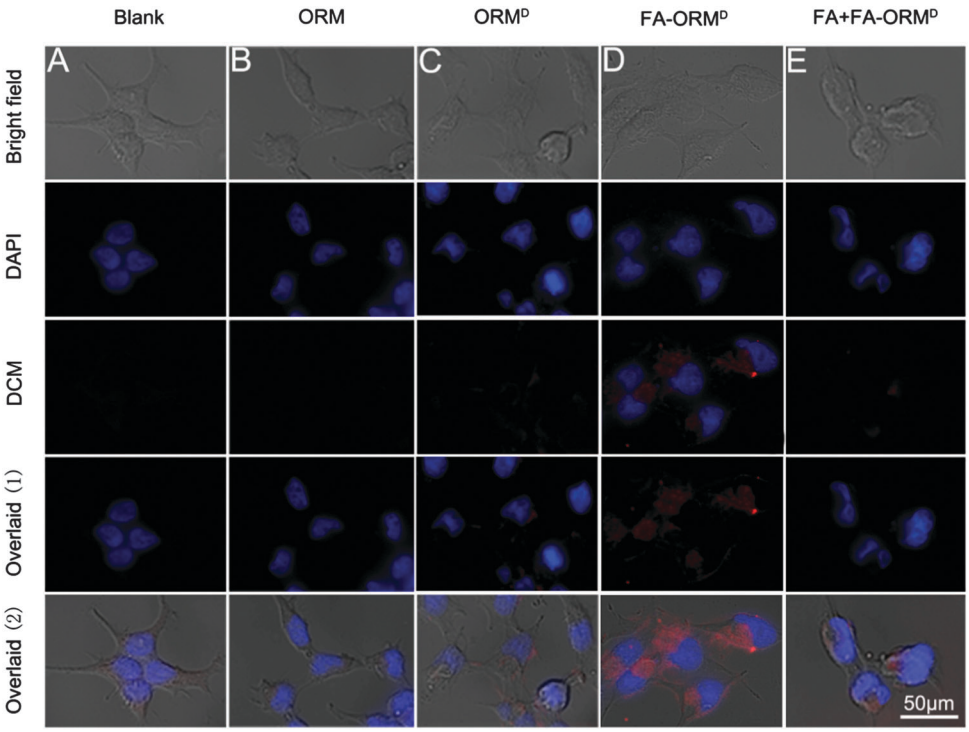

Fig. 2 Fluorescent images of Miapaca-2 cells treated with different ORMSIL nanoparticles. (A) PBS as a blank control, (B) normal ORM nanoparticles as negative controls, (C) ORM^D nanoparticles, and (D) FA-ORM^D nanoparticles. (E) Miapaca-2 cells were pre-treated with FA and then incubated with FA-ORM^D nanoparticles. The cell nucleus was stained with DAPI (pseudo-colored in blue) and signals from DCM were assigned as red. Scale bar is 50 μm.

almost no red fluorescence signals can be detected from 293T cells treated by PBS (Fig. 4A), ORM nanoparticles (Fig. 4B) or FA-ORM^D nanoparticles (Fig. 4D). As shown in Fig. 5, 293T cells treated with ORM^D nanoparticles exhibit obvious fluorescence signals and their corresponding transfection efficiency is estimated to be $28.7 \pm 2.71\%$, which is higher than that of the cells treated with FA-ORM^D nanoparticles (the transfection efficiency is $7.21 \pm 1.32\%$). The above differences demonstrate the specific selectivity of FA-ORM^D nanoparticles for targeting Miapaca-2 cells. As negative controls, the cells treated with ORM or PBS show almost no fluorescence signals from this analysis study. In addition, we incubated other FA-receptor-positive cancer cells (SMMC7721 cells) and FA-receptor-negative cancer cells (MCF7 cells) with ORMOSIL nanoparticles and examined the transfection efficiency by flow cytometry (Fig. S1 and S2, ESI†). The results were consistent with the studies on Miapaca-2 cells and 293T cells. These results further indicate the feasibility of using FA-ORM^D nanoparticles as the tumor targeting optical probes with high efficiency and specificity for potential clinical research applications such as image-guided surgeries.

Cell viability studies of ORMOSIL nanoparticles

The toxicity of nanoparticles has received tremendous attention in the last decade and it has become a major concern for researchers in the biomedical field. Previous studies have shown that semiconductor quantum dots (QDs) are reported to be non-toxic at a relatively high dose (*e.g.* 10^{-9} M for CdTe QDs[57]) and such a dosage is routinely used for optical imaging *in vivo*. More recently, many research groups suggested that such QDs may degrade in the body if they are applied for long-term *in vivo* applications. The degradation of QDs will eventually lead to the release of heavy metals to the body and causing toxicity. This is indeed an important scenario that we need to take precaution of, especially QDs are likely to be accumulated in the liver and spleen after performing their programmed tasks *in vivo*.[58,59] Cationic polymer nanoparticles (*e.g.* poly-L-lysine and polyethyleneimine) are often applied for studying the dynamic interactions between the cell membrane and biomolecules and for understanding the cellular uptake of drug molecules.[60,61] However, the proton sponge effect from these cationic polymer nanoparticles may lead to osmotic swelling, lysosome rupture and induced cell apoptosis.[62] For instance, polyethyleneimine nanoparticles can cause a decrease in the cell metabolic activity by 40–90% at a typical concentration used for the transfection study.[63] The cationic lyposomes (*e.g.* lipofectamine), which is another type of nanoparticles for promoting cell transfection, have been reported to be toxic to cells due to the generation of oxygen radicals from this formulation.[64] Silica nanoparticles are expected to possess low cytotoxicity considering silica is a FDA approved chemical agent for food processing. Even so, silica particles may exhibit some degree of toxicity if their size, shape and surface properties are altered in the nanoscale dimension.[65,66] Therefore, it is essential to evaluate the toxicity of the prepared silica nanoparticles before applying them for other complex experiments that involve further modification of the particles. For our synthesized ORMOSIL nanoparticles, *in vitro*

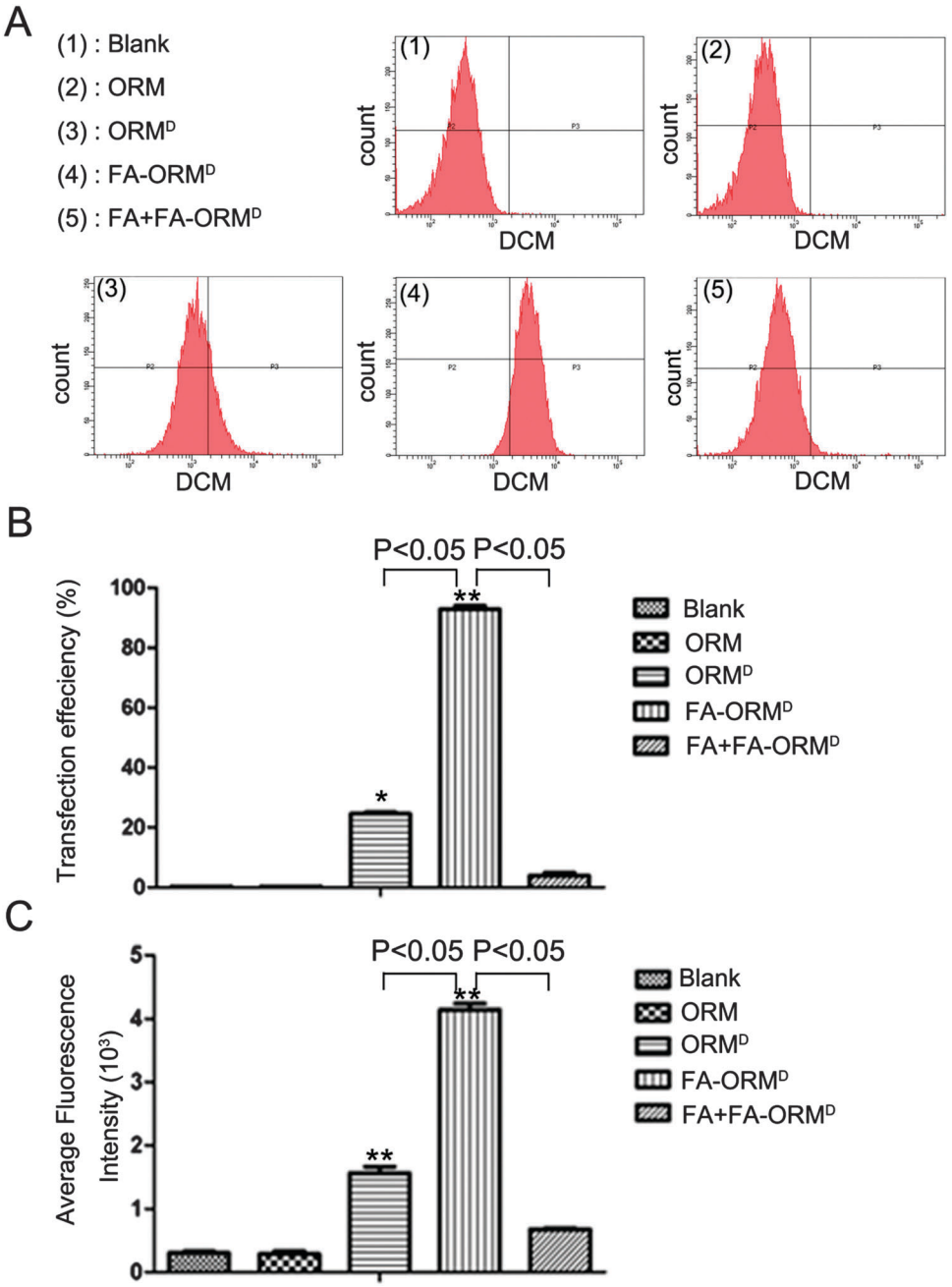

Fig. 3 Transfection efficiency of ORMOSIL nanoparticles in Micapaca-2 cells. (A) Representative dot plots of flow cytometry assays, in which cells were treated with (1) PBS, (2) ORM nanoparticles, (3) ORM^D nanoparticles, (4) FA-ORM^D nanoparticles and (5) FA followed by FA-ORM^D nanoparticles. (B) Transfection efficiency and (C) average fluorescence intensity calculated from the results showed in (A). Values are means ± SEM, $n = 3$; *$P < 0.05$, **$P < 0.01$ *vs.* Blank (PBS) and ORM.

microscopy imaging and MTT assay are performed to examine their toxicity (Fig. 6). In Fig. 6A, Miapaca-2 cells are separately treated with 0.1 mg mL^{-1} (2 times of the average concentration used in fluorescent cell imaging) ORM, ORM^D or FA-ORM^D nanoparticles for 24 h. According to the bright field imaging results, no significant decrease of the cell numbers is observed for cells treated with these three different ORMOSIL nanoparticle formulations. In Fig. 6B, the cell viability of cells treated with three different ORMOSIL nanoparticles is maintained over 80% at a concentration of up to 1 mg mL^{-1}. Therefore, ORMOSIL nanoparticles are non-toxic and suitable to be used for *in vitro* imaging such as drug delivery monitoring in a single cell.

In vivo tumor imaging study

During the last few years, researchers have developed a variety of nanoparticles to specifically target tumor cells by functionalizing their surface with targeting ligands. However, the feasibility of using these nanoparticles for *in vivo* applications remains a

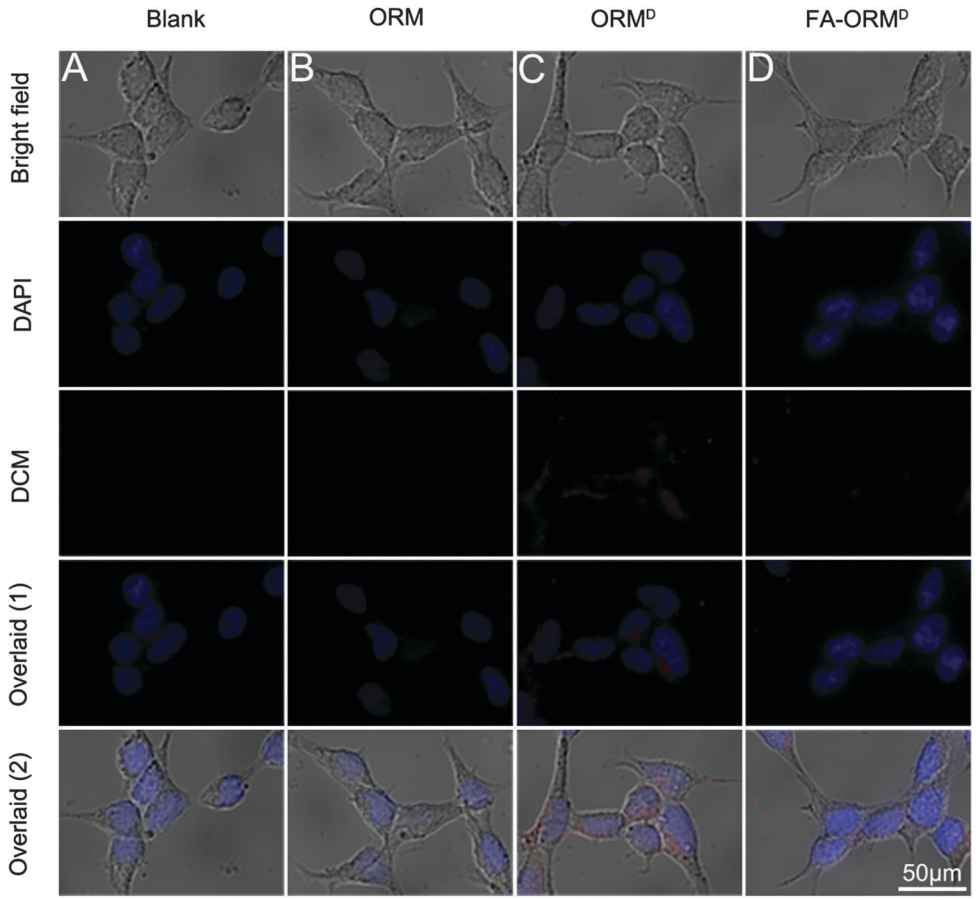

Fig. 4 Fluorescent images of 293T cells treated with different ORMSIL nanoparticles. (A) PBS as a blank control, (B) ORM nanoparticles as negative controls, (C) ORM^D nanoparticles, and (D) FA-ORM^D nanoparticles. The cell nucleus was stained with DAPI (pseudo-colored in blue) and signals from DCM are assigned in red. Scale bar is 50 μm.

challenge as many of these formulations are not stable in the biological environment. To investigate the potential of FA-ORM^D nanoparticles for *in vivo* imaging, the Miapaca-2 tumor-bearing mice are injected with 200 μL FA-ORM^D nanoparticles (1 mg mL^{-1}) by tail vein injection. The mice (n = 3) intravenously injected with FA-ORM^D nanoparticles or PBS (as the control) are imaged at different time points (1 hour, 5 hours, 24 hours and 96 hours) using the IVIS Lumina II small animal *in vivo* optical imaging system (Fig. 7). After an hour of injection, strong fluorescence signals are observed at the tumor site of treated mice while no signal is detected for mice treated with PBS buffer (Fig. 7B). During the next 4 hours, the optical signal intensity increases from tumor *in vivo* (Fig. 7C). The treated mice are further imaged for 96 hours to examine the *in vivo* distribution of FA-ORM^D nanoparticles. There are weak fluorescence signals detected from the tumor after 24 hours of treatment (Fig. 7D) and these signals disappeared after 96 hours (Fig. 7E). The negative control study (Fig. 7A) shows that there are no fluorescence signals from untreated mice. In addition, the treated mice are sacrificed after 2 weeks of post-injection and their major organs such as liver, kidney, lung, spleen, and brain are removed and analyzed with optical imaging system (Fig. 7F and G). From our imaging analysis, weak fluorescence signals are detected from the liver and almost no signals are observed from the lung, brain and kidney. Such an observation is consistent with previous reports on the biodistribution of silica nanoparticles and indicating that majority of the nanoparticles were accumulated in the liver. It is worth mentioning that the specific accumulation of the nanoparticles at the tumor site demonstrates the high specificity of FA-ORM^D nanoparticles for tumor targeting. Moreover, the fluorescence signals can be detected even after 24 hours of injection, which shows the potential of using FA-ORM^D nanoparticles for long-term tumor imaging *in vivo*.

To further evaluate the toxicity of FA-ORM^D nanoparticles *in vivo*, histological analysis was also performed on the major organs of treated mice (Fig. 8). After two weeks, tumor-bearing mice groups (treated with FA-ORM^D nanoparticles or PBS) are sacrificed and their major organs such as heart, liver, spleen, lung, kidney and brain are harvested for analysis. As shown in histological images, no signs of organ lesions are observed from the mice treated with FA-ORM^D nanoparticles as compared to those treated with PBS. Overall, these *in vivo* results provide strong evidence that FA-ORM^D nanoparticles can be an efficient and biocompatible tool for *in vivo* imaging applications.

Pancreatic cancer is a common cancer with high degree of malignancy and an exceptionally high mortality rate, which

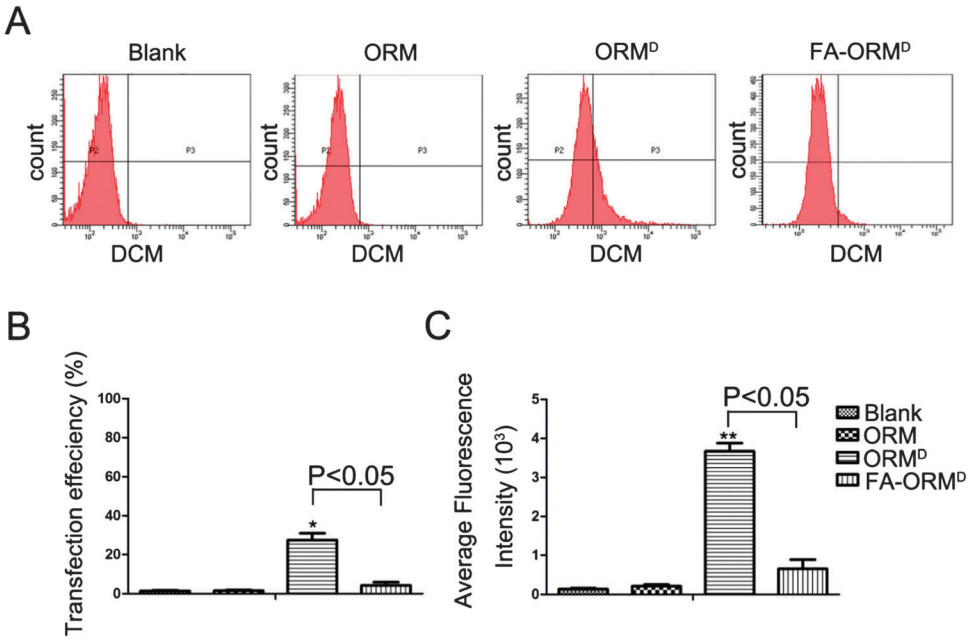

Fig. 5 Transfection efficiency of ORMOSIL nanoparticles in 293T cells. (A) Representative dot plots of flow cytometry assays, in which cells were treated with PBS (as blank), ORM nanoparticles, ORM^D nanoparticles and FA-ORM^D nanoparticles for 4 hours. (B) Transfection efficiency and (C) average fluorescence intensity calculated from the results showed in (A). Values are means ± SEM, $n = 3$; * $P < 0.05$, ** $P < 0.01$ *vs.* Blank (PBS) and ORM.

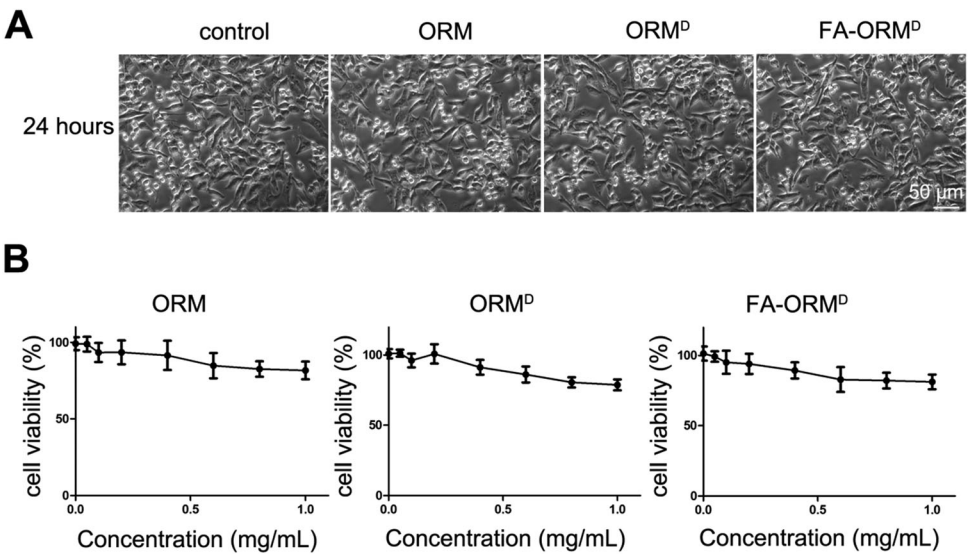

Fig. 6 Cell imaging and cell viability test of different ORMOSIL nanoparticles. (A) Bright field images of Miapaca-2 cells treated with PBS, ORM nanoparticles, ORM^D nanoparticles and FA-ORM^D nanoparticles for 24 hours. Scale bar is 50 μm. (B) Cell viability of Miapaca-2 cells treated with ORM nanoparticles, ORM^D nanoparticles and FA-ORM^D nanoparticles for 24 h ($n = 3$). Percentage cell viability of the treated cells is calculated relative to that of untreated cells (with arbitrarily assigned 100% viability). Data are presented as the means ± SEM of triplicate experiments.

ranks fourth among the causes of cancer-related death in most developing countries. It is very difficult to diagnose pancreatic cancer at an early stage owing to lack of specific symptoms. After primary diagnosis, around 25% survive for one year and only 5% survive for five years. Therefore, the detection and diagnosis of pancreatic cancer in the early stage are urgently needed. The traditional methods for diagnosing pancreatic cancer include computed tomography (CT scan), magnetic resonance imaging (MRI), ultrasound, positron emission tomography (PET scan) and biopsy.[67] These methods can detect the advanced pancreatic cancer but are hardly able to diagnose pancreatic cancer at an early stage. The morphological alterations are detectable by the conventional techniques only when the tumor is larger than 0.5–1 cm.[68] Since the early stage pancreatic carcinoma is small and as such it will be very difficult to be differentiated from inflammatory tissues.

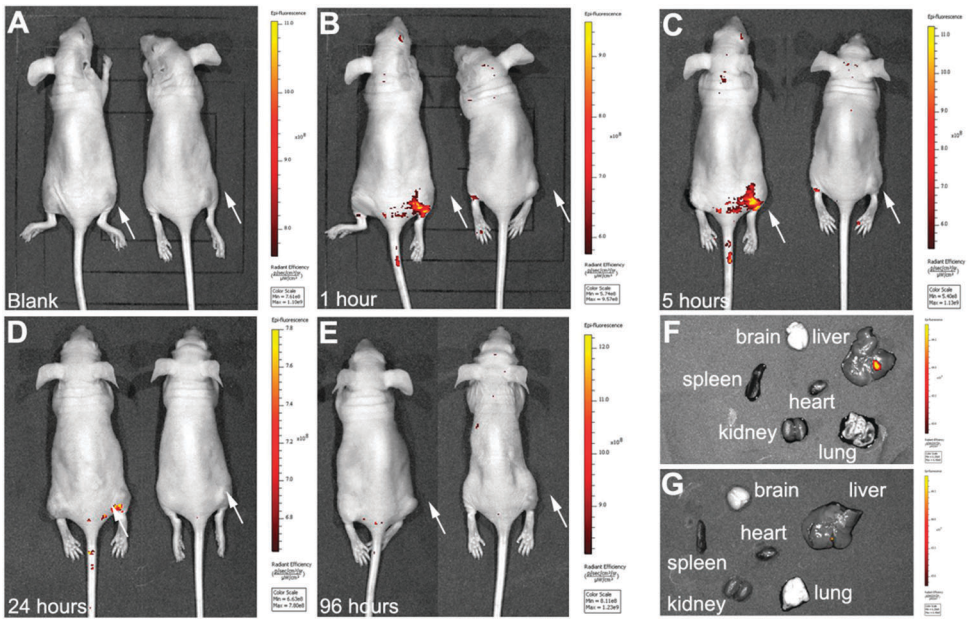

Fig. 7 Time dependent *in vivo* luminescence imaging. (A–E) The Miapaca-2 tumor-bearing mice (pointed by white arrows) were injected with 200 μL of FA-ORM^{D} nanoparticles (1 mg mL^{-1}, the left one) and 200 μL PBS as control (the right one). All images were acquired under the same experimental conditions. (A) Untreated mice as negative controls. (B–E) Fluorescence images of tumor tissues at indicated times after tail vein injection. After two weeks, major organs of mice treated with FA-ORM^{D} nanoparticles (F) or PBS (G) are removed and analyzed using the optical imaging system.

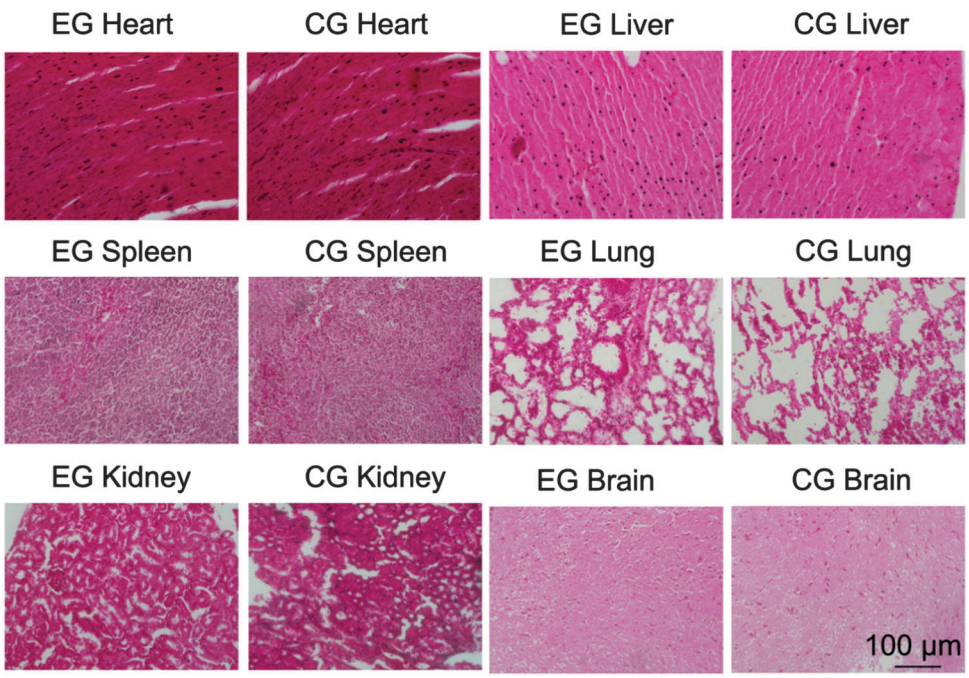

Fig. 8 Histological studies on the major organs of the mice intravenously injected with FA-ORM^{D} nanoparticles or PBS after two weeks. Tissues were harvested from heart, liver, spleen, lung, kidney and brain respectively. EG (experimental group) represents the group treated with FA-ORM^{D} nanoparticles, CG (control group) represents the group treated with PBS.

Benefiting from its high spatial resolution capability, optical imaging is a promising technique for pancreatic cancer detection and diagnosis. With the use of exogenous fluorescence probes (organic fluorophores and nanomaterials) for targeting the surface molecules of pancreatic cancer cells, the change, distribution and metastasis of tumor cells can be readily captured at the early stage. However, the main limitation of optical imaging lies in the low penetration depth of the light. Even for the near-infrared light, it can only penetrate the solid tissues for only several millimetres.[69] Surgical diagnostics will

provide a possible solution to overcome this challenge but it is not cost-effective for early detection and may even promote metastasis. For practical use in early-stage cancer diagnosis, we suggest that optical imaging can be combined with the endoscopic diagnostic tool and optical coherence tomography (OCT) for ultrasensitive detection. An endoscopic approach provides ready access to human tissue and OCT can improve the spatial resolution in 3D imaging.[70,71] QDs can be used as contrast-enhancing agents for these techniques,[72] thereby allowing one to obtain high resolution images of the disease sites. In recent years, nanoparticles have been an advantageous alternative to organic fluorophores because of their robustness, biocompatibility and tuneable size. However, the toxicity of some nanomaterials such as the accumulation of heavy-metal quantum dots in body and *in vivo* immune responses induced by lipid nanoparticles[73] is a major concern for many biomedical researchers and clinicians.

Due to their good biocompatibility and biodegradability, silica nanoparticles are suitable probes for a variety of therapeutic applications ranging from drug delivery[42,74] to optical imaging.[38,43] However, some conventional synthesis processes are complex and time-consuming. In our studies, we prepared fluorescent organically modified silica (ORMOSIL) nanoparticles in a simple oil-in-water microemulsion system with the presence of fluorescence dyes (DCM). This method is facile and straightforward. DCM is selected as the optical dye since it is hydrophobic and preferentially solubilized in the oil droplets of the oil-in-water microemulsion system. In addition, the emission of the organic dye is within the red to near-infrared (NIR) spectral region and thus significantly reduces the background noise during *in vivo* imaging. The ORM^D nanoparticle surface is conjugated with folic acid (FA-ORM^D), which endowed FA-ORM^D nanoparticles with tumor targeting ability. The over-expression of FA receptors is commonly found in most of the epithelial-derived cancer cells type, including ovarian cancer, lung cancer, breast cancer, brain cancer and pancreatic cancer.[75,76] To date, a variety of FA conjugated nanoparticles have been developed to enhance specific targeting of tumors for *in vivo* optical imaging, such as FA-iron oxide nanoparticles,[73] FA-metal nanoparticles[77] and FA-quantum dots.[76] However, the fluorescence signals from these nanoparticles are observed to be diminished within 4 hours of *in vivo* imaging since the larger size ($\sim$100 nm) particles are eliminated from bloodstream in a short period of time (due to the RES system)[78] and smaller size ($<$10 nm) particles are excreted from the body through renal clearance.[69] It is worth mentioning that the fluorescence signals of FA-ORM^D can be maintained for 24 hours, which indicated that the particle size ($\sim$30 nm) is probably suitable for long term *in vivo* imaging applications. Furthermore, the *in vitro* and *in vivo* experiments demonstrated here showcase the excellent tumor targeting ability of FA-ORM^D nanoparticles without causing any damage to the normal tissues. Therefore, FA-ORM^D nanoparticles are expected to be potentially translated for clinical research application of pancreatic tumor targeting and imaging *in vivo.*

Conclusion

In summary, a folic acid-conjugated ORMSIL nanoprobe (FA-ORM^D) with intense fluorescence signals is synthesized with small hydrodynamic size, good biocompatibility and specific tumor targeting ability. The *in vitro* imaging and flow cytometry studies collectively show that FA-ORM^D nanoparticles are preferentially taken up by Miapaca-2 cells and SMMC7721 cells when compared to 293T cells and MCF7 cells. Using the small animal imaging system, we observe specific accumulation of FA-ORM^D nanoparticles at the tumor site after an hour of injection. The accumulation of nanoparticles persisted for 24 hours, which demonstrated the strong specificity and robustness of FA-ORM^D nanoparticles *in vivo*. The cell viability evaluated by MTT assay (80% at 1 mg mL^{-1}) and the major organs (no ill effects in the treated mice) assessed by the histological analysis suggest that these FA-ORM^D nanoparticles are highly biocompatible for *in vivo* applications. Overall, we have developed an efficient and specific nanoprobe (FA-ORM^D) for *in vivo* optical imaging using a simple synthesis protocol. The biocompatibility, low-toxicity and robustness properties of FA-ORM^D nanoparticles may aid biomedical researchers to develop clinical usable functionalized silica nanoparticles for cancer theranostics.

Disclosure

No conflict of interest exists in the submission of this manuscript and none declared.

Acknowledgements

This work was supported by the Singapore Ministry of Education (Grants Tier 2 MOE2010-T2-2-010 (M4020020.040 ARC2/11) and Tier 1 M4010360.040 RG29/10), NTU-NHG Innovation Collaboration Grant (No. M4061202.040), A*STAR Science and Engineering Research Council (No. M4070176.040) and School of Electrical and Electronic Engineering at NTU, National Natural Science Foundation of China (NSFC) (81301318), Shenzhen Basic Research Project (JCYJ20140418182819164, JCYJ20140418091413563) and (JCYJ20140418095735543).

References

1 H. Kobayashi, M. R. Longmire, M. Ogawa and P. L. Choyke, *Chem. Soc. Rev.*, 2011, **40**, 4626–4648.
2 S. R. Meikle, F. J. Beekman and S. E. Rose, *Drug Discovery Technol.*, 2006, **3**, 187–194.
3 K. Y. Jeong, K. Choi, W. H. Nam and J. B. Ra, *Phys. Med. Biol.*, 2011, **56**, 4881.
4 J. L. Vivero-Escoto, R. C. Huxford-Phillips and W. Lin, *Chem. Soc. Rev.*, 2012, **41**, 2673–2685.
5 N. Beckmann, *Braz. J. Phys.*, 2006, **36**, 16–22.
6 K. O. Vasquez, C. Casavant and J. D. Peterson, *PLoS One*, 2011, **6**, e20594.

7 S. Dufort, L. Sancey, C. Wenk, V. Josserand and J. L. Coll, *Biochim. Biophys. Acta, Biomembr.*, 2010, **1798**, 2266–2273.
8 M. van Oosten, T. Schafer, J. A. C. Gazendam, K. Ohlsen, E. Tsompanidou, M. C. de Goffau, H. J. M. Harmsen, L. M. A. Crane, E. Lim, K. P. Francis, L. Cheung, M. Olive, V. Ntziachristos, J. M. van Dijl and G. M. van Dam, *Nat. Commun.*, 2013, **4**, 2584.
9 W. M. Leevy, N. Serazin and B. D. Smith, *Drug Discovery Today: Dis. Models*, 2007, **4**, 91–97.
10 A. P. Patterson, S. A. Booth and R. Saba, *BioMed Res. Int.*, 2014, 401306.
11 M. Bouvet, J. W. Wang, S. R. Nardin, R. Nassirpour, M. Yang, E. Baranov, P. Jiang, A. R. Moossa and R. M. Hoffman, *Cancer Res.*, 2002, **62**, 1534–1540.
12 R. M. Hoffman, *Cell Death Differ.*, 2002, **9**, 786–789.
13 A. Hanyu, K. Kojima, K. Hatake, K. Nomura, H. Murayama, Y. Ishikawa, S. Miyata, M. Ushijima, M. Matsuura, E. Ogata, K. Miyazawa and T. Imamura, *Cancer Sci.*, 2009, **100**, 2085–2092.
14 T. Xiong, Y. J. Li, Z. Y. Li, X. M. Xie and L. S. Lu, *J. Biomed. Nanotechnol.*, 2013, **9**, 274–280.
15 R. Dave, D. S. Terry, J. B. Munro and S. C. Blanchard, *Biophys. J.*, 2009, **96**, 2371–2381.
16 A. R. Katritzky and T. Narindoshvili, *Org. Biomol. Chem.*, 2009, **7**, 627–634.
17 R. Alford, H. M. Simpson, J. Duberman, G. C. Hill, M. Ogawa, C. Regino, H. Kobayashi and P. L. Choyke, *Mol. Imaging*, 2009, **8**, 341–354.
18 U. Resch-Genger, M. Grabolle, S. Cavaliere-Jaricot, R. Nitschke and T. Nann, *Nat. Methods*, 2008, **5**, 763–775.
19 J. Merian, J. Gravier, F. Navarro and I. Texier, *Molecules*, 2012, **17**, 5564–5591.
20 S. Jiang, M. K. Gnanasammandhan and Y. Zhang, *J. R. Soc., Interface*, 2010, **7**, 3–18.
21 M. Levy-Sakin and Y. Ebenstein, *Curr. Opin. Biotechnol.*, 2013, **24**, 690–698.
22 S. K. Saka, A. Vogts, K. Krohnert, F. Hillion, S. O. Rizzoli and J. T. Wessels, *Nat. Commun.*, 2014, **5**, 3664.
23 J. Safari and Z. Zarnegar, *J. Saudi Chem. Soc.*, 2014, **18**, 85–99.
24 S. Bamrungsap, Z. L. Zhao, T. Chen, L. Wang, C. M. Li, T. Fu and W. H. Tan, *Nanomedicine*, 2012, **7**, 1253–1271.
25 K. Park, *ACS Nano*, 2013, **7**, 7442–7447.
26 S. Zeng, D. Baillargeat, H. P. Ho and K. T. Yong, *Chem. Soc. Rev.*, 2014, **43**, 3426–3452.
27 S. Zeng, K.-T. Yong, I. Roy, X.-Q. Dinh, X. Yu and F. Luan, *Plasmonics*, 2011, **6**, 491–506.
28 T. A. Larson, J. Bankson, J. Aaron and K. Sokolov, *Nanotechnology*, 2007, **18**, 325101.
29 C. G. Hadjipanayis, H. B. Jiang, D. W. Roberts and L. Yang, *Semin. Oncol.*, 2011, **38**, 109–118.
30 M. Solomon, Y. Liu, M. Y. Berezin and S. Achilefu, *Med Prin Pract*, 2011, **20**, 397–415.
31 J. J. Lee, A. G. White, D. R. Rice and B. D. Smith, *Chem. Commun.*, 2013, **49**, 3016–3018.
32 J. Harrison, C. A. Bartlett, G. Cowin, P. K. Nicholls, C. W. Evans, T. D. Clemons, B. Zdyrko, I. A. Luzinov, A. R. Harvey, K. S. Iyer, S. A. Dunlop and M. Fitzgerald, *Small*, 2012, **8**, 1579–1589.
33 L. Costantino and D. Boraschi, *Drug Discovery Today*, 2012, **17**, 367–378.
34 L. Wang and W. Tan, *Nano Lett.*, 2006, **6**, 84–88.
35 H. S. Muddana, T. T. Morgan, J. H. Adair and P. J. Butler, *Nano Lett.*, 2009, **9**, 1559–1566.
36 J. Qian, D. Wang, F. Cai, Q. Zhan, Y. Wang and S. He, *Biomaterials*, 2012, **33**, 4851–4860.
37 J. Qian, Y. Wang, X. Gao, Q. Zhan, Z. Xu and S. He, *J. Nanosci. Nanotechnol.*, 2010, **10**, 1668–1675.
38 R. Kumar, I. Roy, T. Y. Hulchanskyy, L. N. Goswami, A. C. Bonoiu, E. J. Bergey, K. M. Tramposch, A. Maitra and P. N. Prasad, *ACS Nano*, 2008, **2**, 449–456.
39 K. M. Wang, X. X. He, X. H. Yang and H. Shi, *Acc. Chem. Res.*, 2013, **46**, 1367–1376.
40 J. Qian, X. Li, M. Wei, X. W. Gao, Z. P. Xu and S. L. He, *Opt. Express*, 2008, **16**, 19568–19578.
41 H. Mader, X. H. Li, S. Saleh, M. Link, P. Kele and O. S. Wolfbeis, *Ann. NY Acad. Sci.*, 2008, **1130**, 218–223.
42 I. Roy, P. Kumar, R. Kumar, T. Y. Ohulchanskyy, K. T. Yong and P. N. Prasad, *RSC Adv.*, 2014, **4**, 53498–53504.
43 F. Barandeh, P. L. Nguyen, R. Kumar, G. J. Iacobucci, M. L. Kuznicki, A. Kosterman, E. J. Bergey, P. N. Prasad and S. Gunawardena, *PLoS One*, 2012, **7**, e29424.
44 C. Caltagirone, A. Bettoschi, A. Garau and R. Montis, *Chem. Soc. Rev.*, 2015, DOI: 10.1039/C4CS00270A.
45 F. Yin, C. Yang, Q. Wang, S. Zeng, R. Hu, G. Lin, J. Tian, S. Hu, R. F. Lan, H. S. Yoon, F. Lu, K. Wang and K. T. Yong, *Theranostics*, 2015, **5**, 818–833.
46 G. Lin, X. Wang, F. Yin and K. T. Yong, *Int. J. Nanomed.*, 2015, **10**, 335–345.
47 A. F. Metaxa, E. K. Efthimiadou, N. Boukos, E. A. Fragogeorgi, G. Loudos and G. Kordas, *J. Colloid Interface Sci.*, 2014, **435**, 171–181.
48 C. P. Leamon, *Curr. Opin. Invest. Drugs (BioMed Cent.)*, 2008, **9**, 1277–1286.
49 P. S. Low and S. A. Kularatne, *Curr. Opin. Chem. Biol.*, 2009, **13**, 256–262.
50 Z. Y. He, Y. Y. Yu, Y. Zhang, Y. D. Yan, Y. Zheng, J. He, Y. M. Xie, G. He, Y. Q. Wei and X. R. Song, *J. Biomed. Nanotechnol.*, 2013, **9**, 833–844.
51 R. Meier, T. D. Henning, S. Boddington, S. Tavri, S. Arora, G. Piontek, M. Rudelius, C. Corot and H. E. Daldrup-Link, *Radiology*, 2010, **255**, 527–535.
52 G. L. Zwicke, G. A. Mansoori and C. J. Jeffery, *Nano Rev.*, 2012, **3**, 18496.
53 Z. J. Zhou, C. L. Zhang, Q. R. Qian, J. B. Ma, P. Huang, X. Zhang, L. Y. Pan, G. Gao, H. L. Fu, S. Fu, H. Song, X. Zhi, J. Ni and D. X. Cui, *J. Nanobiotechnol.*, 2013, **11**, 17.
54 H. Meng, J. Y. Chen, L. Mi, P. N. Wang, M. Y. Ge, Y. Yue and N. Dai, *J. Biol. Inorg. Chem.*, 2011, **16**, 117–123.
55 D. A. Li, Y. T. Zhang, M. Yu, J. Guo, D. Chaudhary and C. C. Wang, *Biomaterials*, 2013, **34**, 7913–7922.
56 Q. Lu, X. Wang, H. Zhu and D. L. Kaplan, *Acta Biomater.*, 2011, **7**, 2782–2786.

57 B. R. Prasad, N. Nikolskaya, D. Connolly, T. J. Smith, S. J. Byrne, V. A. Gérard, Y. K. Gun'ko and Y. Rochev, *J. Nanobiotechnol.*, 2010, **8**, 7.
58 L. Ye, K.-T. Yong, L. Liu, I. Roy, R. Hu, J. Zhu, H. Cai, W.-C. Law, J. Liu and K. Wang, *Nat. Nanotechnol.*, 2012, **7**, 453–458.
59 Y. Zhang, Y. Zhang, G. Hong, W. He, K. Zhou, K. Yang, F. Li, G. Chen, Z. Liu and H. Dai, *Biomaterials*, 2013, **34**, 3639–3646.
60 E. Igarashi, *Toxicol. Appl. Pharmacol.*, 2008, **229**, 121–134.
61 N. Nafee, M. Schneider, U. F. Schaefer and C.-M. Lehr, *Int. J. Pharm.*, 2009, **381**, 130–139.
62 T. Xia, M. Kovochich, M. Liong, J. I. Zink and A. E. Nel, *ACS Nano*, 2007, **2**, 85–96.
63 M. L. Forrest, J. T. Koerber and D. W. Pack, *Bioconjugate Chem.*, 2003, **14**, 934–940.
64 S. Dokka, D. Toledo, X. Shi, V. Castranova and Y. Rojanasakul, *Pharm. Res.*, 2000, **17**, 521–525.
65 Y. Ye, J. Liu, M. Chen, L. Sun and M. Lan, *Environ. Toxicol. Pharmacol.*, 2010, **29**, 131–137.
66 J.-S. Chang, K. L. B. Chang, D.-F. Hwang and Z.-L. Kong, *Environ. Sci. Technol.*, 2007, **41**, 2064–2068.
67 A. Riker, S. K. Libutti and D. L. Bartlett, *J. Surg. Oncol.*, 1997, **6**, 157–169.
68 J. von Burstin, S. Eser, B. Seidler, A. Meining, M. Bajbouj, J. Mages, R. Lang, A. J. Kind, A. E. Schnieke and R. M. Schmid, *Int. J. Cancer*, 2008, **123**, 2138–2147.
69 H. S. Choi, W. Liu, P. Misra, E. Tanaka, J. P. Zimmer, B. Itty Ipe, M. G. Bawendi and J. V. Frangioni, *Nat. Biotechnol.*, 2007, **25**, 1165–1170.
70 N. Fujita, Y. Noda, G. Kobayashi, K. Kimura and K. Ito, *Pancreas*, 2004, **28**, 279–281.
71 E. Zagaynova, O. Streltzova, N. D. Gladkova, N. M. Shakhova, F. I. Feldchtein, V. A. Kamensky, G. V. Gelikonov and E. Donchenko, *J. Clin. Oncol.*, 2004, **22**, 4538, DOI: 10.1117/12.530794.
72 C. Xu, J. Ye, D. L. Marks and S. A. Boppart, *Opt. Lett.*, 2004, **29**, 1647–1649.
73 W. C. Chen, J. P. May and S. D. Li, *Nanotechnol. Rev.*, 2013, **2**, 201–213.
74 A. Gupta, L. N. Goswami, M. Ethirajan, J. Missert, K. V. R. Rao, T. Ohulchanskyy, I. Roy, J. Morgan, P. N. Prasad and R. K. Pandey, *J. Porphyrins Phthalocyanines*, 2011, **15**, 401–411.
75 C. Muller and R. Schibli, *J. Nucl. Med.*, 2011, **52**, 1–4.
76 R. Hu, W. C. Law, G. Lin, L. Ye, J. Liu, J. L. Reynolds and K. T. Yong, *Theranostics*, 2012, **2**, 723–733.
77 M. Fani, M. L. Tamma, G. P. Nicolas, E. Lasri, C. Medina, I. Raynal, M. Port, W. A. Weber and H. R. Maecke, *Mol. Pharmaceutics*, 2012, **9**, 1136–1145.
78 T. Neuberger, B. Schopf, H. Hofmann, M. Hofmann and B. von Rechenberg, *J. Magn. Magn. Mater.*, 2005, **293**, 483–496.